



Article

Prediction of the Bond Strength of Externally Bonded FRP Sheets Applied to Concrete via Grooves Technique Using Artificial Neural Networks

Abdelatif Salmi

Department of Civil Engineering, College of Engineering, Prince Sattam Bin Abdulaziz University, Alkharj 11942, Saudi Arabia; a.salmi@psau.edu.sa

Abstract: The present study aims to fill a gap in the literature on the estimation of the bond strength of fiber reinforced polymer sheets bonded to concrete, via the externally bonded reinforcement on grooves (EBROG) technique, employing the curve-fitting on existing datasets in the literature and the methodology of Artificial Neural Networks (ANNs). Therefore, a dataset of 39 experimental results derived from EBROG technique is collected from the literature. A mathematical equation for the bond strength of FRP sheets applied on concrete via the EBROG technique was suggested using curve-fitting and general regression. The proposed mathematical equation is compared and validated with experimental results. The developed ANN model was constructed after testing diverse hidden layers and neurons to find the optimal predictions. The validation of the model is carried out using the experimental results and a statistical analysis is applied to assess the proposed mathematical equation and the proposed ANN model. Furthermore, a parametric study using the ANN model was also performed to investigate the influence of various factors on the bond strength of FRP sheets bonded to concrete. The parametric study proves that the bond strength increases with increasing the tensile stiffness per width, the FRP sheet width, and the concrete compressive strength; however, the effect of the Groove's width and depth is found to be not monotonous.

Keywords: ANN model; bond strength; EBROG; FRP; mathematical equation



Citation: Salmi, A. Prediction of the Bond Strength of Externally Bonded FRP Sheets Applied to Concrete via Grooves Technique Using Artificial Neural Networks. *J. Compos. Sci.* **2024**, *8*, 30. <https://doi.org/10.3390/jcs8010030>

Academic Editor: Francesco Tornabene

Received: 6 November 2023

Revised: 30 December 2023

Accepted: 9 January 2024

Published: 12 January 2024



Copyright: © 2024 by the author. Licensee MDPI, Basel, Switzerland. This article is an open access article distributed under the terms and conditions of the Creative Commons Attribution (CC BY) license (<https://creativecommons.org/licenses/by/4.0/>).

1. Introduction

While several techniques are used to strengthen and repair reinforced concrete buildings, externally fastened fiber-reinforced polymer (FRP) plates or sheets have become a popular approach. Their many benefits—such as their high tensile strength, remarkable corrosion resistance, and lightweight and flexible nature—have led to this favor. External reinforcement in the form of FRP composite sheets is frequently used to improve the flexural capabilities of beams [1]. However, in a complex interaction impacted by multiple elements, the behavior of the bond formed between the FRP sheet and the concrete surface plays a crucial role in the efficacy of the reinforced structures. The performance of the bond strongly depends on many variables including the concrete's compressive strength, the largest aggregate's size, the FRP material's tensile strength, thickness, modulus of elasticity, adhesive tensile strength, the FRP's length and width, the laborers' level of experience, and the state of the concrete surface. Here, "bond strength" refers to the highest load that the FRP sheet can bear when firmly fastened to the concrete [2].

The early debonding of the FRP from the substrate before the FRP sheet achieves its ultimate bearing capacity is a crucial factor affecting the success of the reinforcing process [3]. There are continuing research investigations on a number of the specifications of FRP composites [4,5] and a wide range of experimental, analytical, and numerical models for bond strength and effective bond length have been developed to date by researchers [4,6–10] and have been approved by various national laws [11] to streamline the design processes for external reinforcement (EBR)-based structural reinforcement of

prepared members. In order to forecast the debonding behavior of RC members reinforced with externally bonded FRP, fracture mechanics techniques have been researched [12–14].

Numerous experimental studies have been conducted to address the bonding issues between the concrete surface and FRP panels. In 2009, Ozbakkaloglu and Saatcioglu [15] employed FRP anchors to resolve delamination problems encountered with surface-bonded FRP sheets. Their research revealed that the use of FRP stabilizers can enhance pull-out capabilities, consequently mitigating the delamination of externally bonded FRP sheets. In 2018, Murad [16] found that the orientation angle of and carbon fiber-reinforced polymer (CFRP) sheets significantly impacts the maximum load and deflection of reinforced concrete elements. Additionally, Ozbacaloglu et al. [17], in their 2017 study, explored the influence of the configuration of FRP anchors on the behavior of externally bonded FRP sheets on concrete structures. They observed that both the number and arrangement of anchors can significantly affect the sliding load behavior of FRP panels. The variables that significantly impact the bond strength between concrete and CFRP panels have been the subject of several experimental studies. Al-Rousan et al.'s research from 2015 [18] showed that while aggregate size has a minor impact on bond strength, the kind of aggregate had a negligible impact. Additionally, they reported that the bond strength increases by increasing concrete compressive strength. They have also found that the bond strength increases by decreasing w/c ratio. Additionally, they discovered that when bond length and width increase, bond strength diminishes. The bonding strength between fibers and concrete is negatively impacted by high temperatures above 400 °C, as Haddad et al. [19] found in 2013, leading to a 64% loss in bond strength. Finally, in 2016, Irshidat and Al-Saleh [20] discovered that bond length and width affect the behavior of the bond between concrete and fibers.

Despite being widely used, the early debonding of the FRP sheet from the substrate causes problems for the EBR technology in terms of efficient load transfer between concrete and the composite [21–24]. Mostofinejad and Mahmoudabadi have recently introduced a novel method called “externally bonded reinforcement on grooves” as an alternative to the usual EBR surface preparation methodology [25] in order to solve this significant constraint. Using this novel method, the concrete surface where the FRP sheet is to be attached is grooved, and the grooves are then filled with epoxy resin. This innovative method transfers the interfacial stresses in reinforced elements to deeper concrete layers, delaying or eliminating FRP debonding altogether. Consequently, the EBROG method outperforms the conventional EBR. To highlight the benefits of EBROG and investigate its possible uses, a great deal of study and experimentation has been done. Longitudinal grooves have been found to be more efficient than transverse or diagonal ones [25]. The EBR or EBROG approach was used to build reinforced concrete (RC) beams and strengthen them against shear loads in a 2013 study by Mostofinejad and Tabatabaei Kashani [22]. Because FRP strips were affixed to vertical grooves on the lateral edges of the beams, the failure mode shifted from shear to flexural, and the load capacity of the beam increased as a result. In a follow-up study, Mostofinejad and Moghaddas (2014) [23] contrasted the EBR and EBROG methods for flexural reinforcement of specimens of RC beams with different internal steel ratios. The findings showed that under various flexural failure modes, EBROG specimens showed greater maximum load capacity and ductility. In order to ascertain the optimal length and location for longitudinal grooves on the tensile side of RC beams, Mostofinejad and Khozaei [26] experimented with several layouts in 2015. Additionally, utilizing particle image velocimetry (PIV) and the single lap-shear test, research has investigated FRP bond strength, effective bond length, and bond-slip curves [27–29]. In a study employing non-reinforced masonry structures in 2014, Hosseini et al. [24] discovered that the EBROG technique was more effective than the EBR technique at improved external strengthening by utilizing the tensile capacity of CFRP composites.

Worksheets, curve-fitting methods, and a small collection of test results were used to create the current bond strength formulae [16]. As a result, it was difficult for researchers to take into consideration all possible linkages and combinations of components, which made it difficult to create an exact equation. One of the first structural engineering applications

of ML was carried out by Adeli and Yeh in 1989 using artificial neural network (ANN) to design steel beams [30]. Because machine learning models work well in speech recognition, image recognition, and language processing, they are quickly spreading to other technical domains [31]. In the next two decades, unanticipated and revolutionary effects on the entire field of designing and analyzing composite materials and structures can be expected due to the convergence of unprecedented data growth from experiments and simulations, increasing computing power, and developing advanced algorithms [31].

Artificial Neural Networks (ANN) have been the most widely used machine learning model in recent years. Based on experimental data, these ANN models are frequently used to explain events in complicated systems when a thorough physical knowledge is unavailable [32]. ANN has found use in a variety of engineering challenges, in contrast to traditional methods based on continuum mechanics. This pattern has been used in the design of steel constructions and for one-dimensional stress states in tension tests of metal specimens at elevated temperatures [33,34]. In [35–39], ANNs have been used to characterize the vibrations of structures, stability problems in structures, reliability studies of structures, and the effect of welding on material characteristics. Furthermore, an ANN was suggested for steel pressure vessel embrittlement, specifically with reference to nuclear reactors [40]. In [41], multiscale issues were discussed. ANNs have the advantage of being able to completely replace mechanical models and drastically reduce computing time. It is not necessary to specify material properties because they can be taught exclusively on experimental data [42]. As a result, a mathematical model based on neural networks is created that can approximate any given function [43]. This method approximates the intended output data by refining all parameters, including weights and biases, using a supervised learning algorithm [44]. User-provided examples and experiences direct the ANN's learning process [45].

There is still no formula to predict the bond strength between concrete and FRP as a function of influencing factors, despite some experimental programs and analytical models focusing on the factors influencing the bond strength between FRP sheets and concrete surfaces when using EBROG. Furthermore, little study has been conducted on the application of ANN equations to determine the bonding strength of FRP sheets adhered to concrete using the EBROG approach.

Setting the standards for FRP's use in structural composites is essential to determining the bonding strength at the concrete-FRP interface. With the use of a sizable testing dataset, this study attempts to present a unique mathematical formula and ANN model for evaluating the binding strength of FRP sheets applied to concrete using the EBROG approach. The main goal is to use curve-fitting and a general regression method in the MATLAB program to determine the best form for a projected mathematical equation. Then, in order to obtain the greatest fit, an ANN model is suggested and calibrated using the testing dataset. Additionally, a thorough parametric study is carried out utilizing the projected ANN equation in order to evaluate the impact of different factors on bond strength.

2. Dataset Development

Moghaddas et al. (2019) experimentally investigated the FRP-concrete bond strength for ERBOG subjected to the single lap-shear test [3]. The image processing technique of PIV was used to analyze the strain and stress fields on the FRP bond area. Table 1 exhibits the characteristics of the 39 specimens prepared through the EBROG technique. Specimens' specifications include groove's width (b_g) and depth (h_g), FRP sheet width (b_f) and tensile stiffness per width (E_{ft}), and concrete compressive strength (f_c). The precision of the outcomes was guaranteed through the execution of a minimum of one additional iteration for each test, resulting in a noticeable reduction in the variability of experimental results. This enhancement in consistency significantly bolstered the robustness and confidence level of the findings.

Table 1. Specimen specifications and the experimental results [3].

b_g (mm)	h_g (mm)	E_{ftf} (kN/mm)	b_f (mm)	f_c (MPa)	P (kN)
5	5	12.92	40	37.88	6.91
5	5	12.92	50	27.09	7.87
5	5	12.92	60	32.7	10.15
5	5	25.3	30	39.07	7.15
5	5	25.3	40	22.68	9.4
5	5	25.3	60	28.09	11.85
5	5	39.1	30	26.69	8.56
5	5	39.1	50	32.7	14.75
5	5	78.2	30	39.07	11.44
5	5	78.2	40	22.68	16.1
5	10	12.92	40	22.68	7.37
5	10	12.92	60	26.67	9.51
5	10	25.3	30	26.69	7.2
5	10	25.3	30	48.15	7.59
5	10	39.1	30	39.07	9.32
5	10	39.1	40	22.68	10.95
5	10	39.1	60	32.7	16.64
10	10	12.92	40	22.68	7.68
10	10	12.92	50	48.24	8.51
10	10	12.92	60	45.35	9.1
10	10	25.3	40	37.88	9.69
10	10	25.3	60	47.9	12.67
10	10	39.1	30	39.07	8.72
10	10	39.1	40	22.68	10.96
10	10	39.1	40	47.9	10.42
10	10	39.1	50	36.46	14.45
10	10	39.1	60	26.67	15.31
10	10	78.2	30	26.69	12.93
10	10	78.2	30	48.15	11.49
10	10	78.2	50	47.9	16.71
10	10	78.2	60	48.24	19.05
10	15	12.92	40	37.88	7.43
10	15	12.92	60	36.94	10.12
10	15	12.92	60	45.35	9.12
10	15	25.3	50	27.09	11.01
10	15	39.1	50	27.09	12.66
10	15	39.1	60	45.35	14.94
10	15	78.2	40	37.88	16.71
10	15	78.2	60	28.09	20.01

The statistical details of these characteristics and the bond strengths obtained from the strain and stress profiles for all the EBROG are given in Table 2.

Table 2. Dataset information of bond strength of FRP sheets applied on concrete via EBROG technique.

	b_g (mm)	h_g (mm)	E_{ftf} (kN/mm)	b_f (mm)	f_c (MPa)	P (kN)
Lowest	5	5	12.92	30	22.68	6.91
Highest	10	15	78.2	60	48.24	20.01
Mean	7.89	9.87	37.54	45.79	34.76	11.46
St. deviation	2.51	3.43	23.57	11.65	9.14	3.54
Coef. of variance	0.32	0.35	0.63	0.25	0.26	0.31

3. Projected Mathematical Equation

In the scientific literature, some equations have been developed to estimate the effective bond length for externally bonded reinforcement on grooves, but there is no proposed mathematical equation to predict the bond strength. One of the objectives of this paper is

to develop an accurate equation that can be used to predict the bond strength for externally bonded reinforcement on grooves.

In our research, data from reference [3] have been used and curve-fitting on the data has been performed. The general form of the formula is taken similar to the equation proposed by Moghaddas et al. (2019) [3], for the effective bond length of FRP sheets bonded on concrete, through the EBROG technique, which depicted the highest precision as compared with the other equations suggested by other researchers [46–49].

The overall organization of the currently forecasted equation for the bond strength for the FRP sheet is shown in Equation (1).

$$P = \alpha (E_{ftf})^{\beta_1} (f'_c)^{\beta_2} \exp(\gamma_1 h_g + \gamma_2 b_g + \gamma_3 b_f) \tag{1}$$

MATLAB’s curve fitting method was employed to acquire the best fit to the testing dataset, yielding counts for the constants α , β_1 , β_2 , γ_1 , γ_2 and γ_3 of 1.57, 0.41, -0.08 , 0.002, 0.002 and 0.017, correspondingly. Consequently, below is the equation predicting the bond strength of FRP sheets applied on concrete, through the EBROG technique.

$$P = 1.57 (E_{ftf})^{0.41} (f'_c)^{-0.08} \exp(0.002(h_g + b_g) + 0.017b_f) \tag{2}$$

The forecasted equation for the bond strength was evaluated employing the dataset presented in Table 1. The factor of determination (R^2) and the root mean square error ($RMSE$) which are provided by Equations (3) and (4), the most significant statistical measures and the most suited to account for testing data, were utilized in this comparative investigation.

$$R^2 = \frac{n(\sum_{i=1}^n x_i y_i) - (\sum_{i=1}^n x_i)(\sum_{i=1}^n y_i)}{[n\sum_{i=1}^n x_i^2 - (\sum_{i=1}^n x_i)^2][n\sum_{i=1}^n y_i^2 - (\sum_{i=1}^n y_i)^2]} \tag{3}$$

$$RMSE = \sqrt{\frac{1}{n} \sum_{i=1}^n (x_i - y_i)^2} \tag{4}$$

Here n indicates the number of tested elements, x_i is the target secured from experiments and y_i is the value given by the mathematical equation. Figure 1 shows the assessment of the mathematical equation.

Figure 1 shows that the forecasted equation given by Equation (2) performed well and it is observed that the projected equation depicted high precision with $R^2 = 0.954$ and $RMSE = 0.0641$ as compared with experimental results. The accuracy of the developed equation can be seen through the absolute error value for each individual measurement, which is obtained in the majority of experimental results within 10%.

Figure 2 plots the distribution of the bond strength of FRP sheets bonded on concrete through the EBROG method both experimentally measured and predicted using the proposed mathematical equation.

In Figure 2, the distribution of the bond strength, both experimentally measured and predicted, is shown. Figure 2 clearly shows that eleven values of the measured bond strengths are between 6 and 9 kN. On the other hand, the suggested equation predicted nine values within this range. In the interval 9–12 kN, there were 15 testing and 16 predicted values; in the 12–15 kN limit, there were 6 testing and 8 predicted values; in the 15–18 kN limit, there were 5 testing and 4 predicted values. Finally, the experimentation and the proposed equation give the same number of values in the range 18–21 kN; there were two testing and two forecasted values. These quantities further demonstrate that the projected model precisely captured the bond strength of FRP sheets applied to concrete through the EBROG technique.

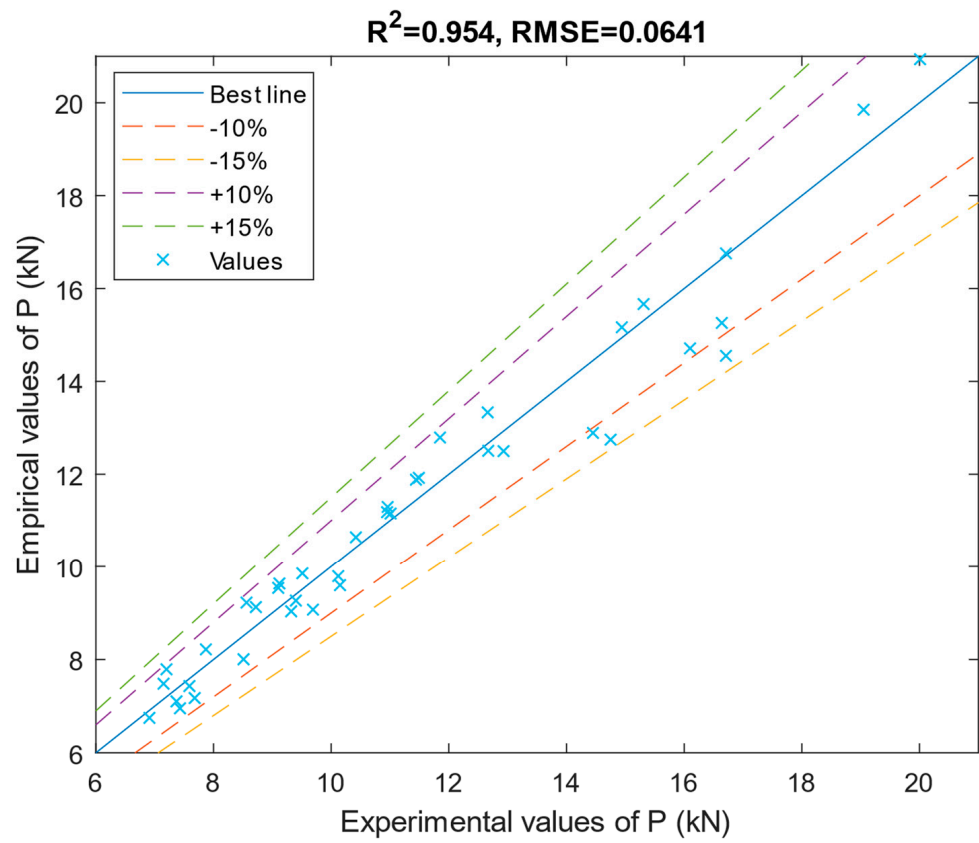


Figure 1. Assessment of the mathematical equation.

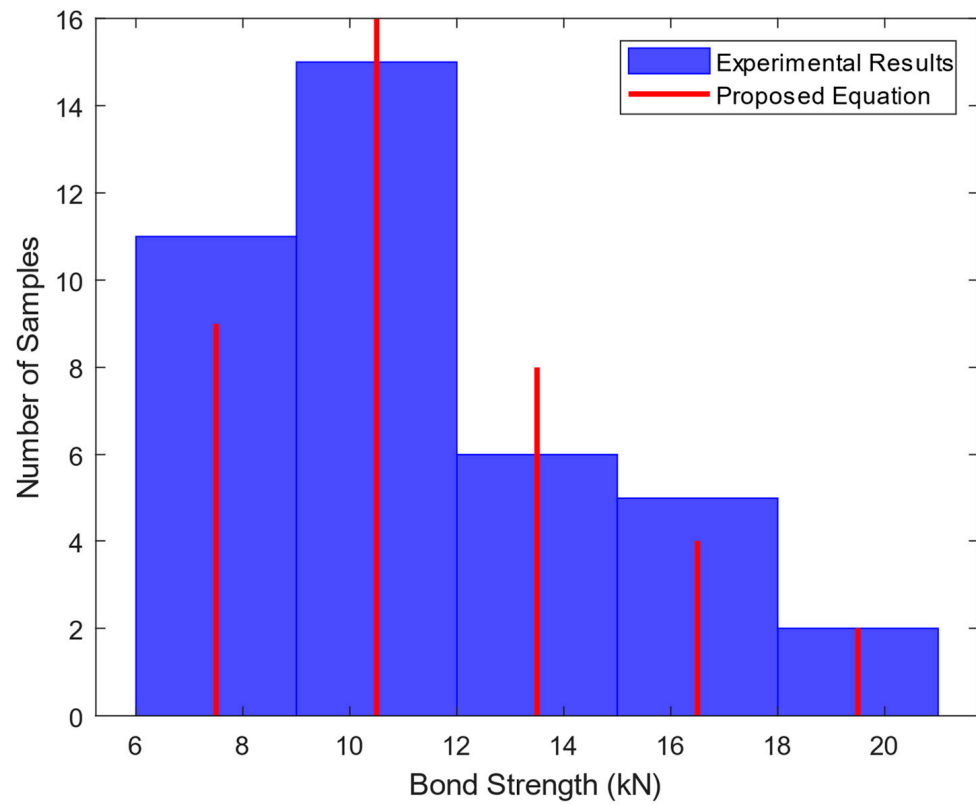


Figure 2. Histograms of experimental and predicted results.

4. Artificial Neural Networks

ANNs have the ability to compress, simplify, categorize, and imagine the counts of many complicated factors. They consist of a number of layers, each of which contains a cluster of integrated “neurons”. All neurons are connected by a link that has a certain weight. The counts provided by the neurons are multiplied by these particular weights. Links are taken to transmitting the outcomes of the previous phase, adding bias [50]. This resulting total serves as the input to an activation function that displays the connection between the several levels as defined by Equation (5).

$$Output = f\{\sum w_i x_i + b\} \tag{5}$$

Here, w_i represents the constants of weight, x_i represents the counts provided as input, and b represents the bias quantity. Neurons in the below-given layer obtain counts from the activation function as input. The bond strength is forecasted by employing ANNs throughout the current experiment. In ANNs, features of the material and geometry of FRP sheets and the grooves are always transported in an input layer (IL). In the present investigation, five factors are defined as the inputs to ANN equations such as the groove’s width and depth, FRP sheet width, the tensile stiffness per width, and the concrete compressive strength. As more relationships are carried across the data to connect the provided factors to one another and to the output factors, the counts from the IL progress to the hidden layer (HL). The construction of the neural networks in ANNs determines how many HLs are taken to process input [50]. The output, the bond strength, is the last one. The specified activation function has a considerable impact on the output efficacy and functionality of the ANNs model. From the left to the right side of the ANN structure, the signals generated by the diverse IL neurons are handled before being sent to the OL on the right side of ANN assemblies [51]. The IL, hidden, and OL of the ANN equations were taken to analyze the testing data of FRP sheets/concrete bond strength. Sigmoid functions were taken as the predetermined activation functions. In order to correct randomly chosen counts provided to weights at the beginning, the key goal of this repeating procedure is to confidently match the outcomes with the final counts in order to attain the highest level of output precision minimizing output error in the form of the factor of determination (R^2) and the root mean square error (RMSE).

4.1. Normalization of Dataset

The accuracy and simplicity of the expected ANN model are also significantly influenced by the normalization procedure. Because diverse factors have diverse units, the normalizing approach enables their transformation to unitless factors. To prevent the issues caused by the poor learning scopes of ANN at the highest and lowest counts, the supplied counts of the factors should be controlled between the appropriate ultimate value of the factors (LeCun et al., 2012) [52]. All of the factors related to the bond strength between FRP sheets and concrete are between 0 and 1, as shown in Table 3.

Table 3. Equations for the normalized quantities.

Quantities	Normalized Quantities
Groove width : b_g	$b_{g\,norm} = \frac{b_g - b_{g\,min}}{b_{g\,max} - b_{g\,min}}$
Groove thickness : h_g	$h_{g\,norm} = \frac{h_g - h_{g\,min}}{h_{g\,max} - h_{g\,min}}$
Product of thickness and elasticity modulus of FRP sheets : $E_f t_f$	$E_f t_{f\,norm} = \frac{E_f t_f - E_f t_{f\,min}}{E_f t_{f\,max} - E_f t_{f\,min}}$
Width of FRP sheets : b_f	$b_{f\,norm} = \frac{b_f - b_{f\,min}}{b_{f\,max} - b_{f\,min}}$
Compression stress of concrete: f'_c	$f'_{c\,norm} = \frac{f'_c - f'_{c\,min}}{f'_{c\,max} - f'_{c\,min}}$

The constructed dataset is split into two separate sets, with 70% of the dataset taken to train the ANN model and 30% of the dataset taken to validate and test it.

4.2. Structure of ANN Model

In the structure of the ANN model, the kind of activation function, the number of neurons in each layer, and the number of internal layers have a significant impact on estimation correctness. This kind of problem determines the ANN's design, which is then refined through a process of trial and error. The number of neurons and HL is significantly determined by the issue type, input data, and existing dataset. In this research, a MATLAB code is developed to fix the internal and hyperparameters of the ANN model. The code allows the investigation of the effect of the number of layers and neurons on the factor of determination (R^2) and the root mean square error (RMSE). The Selected ANN model corresponds to the maximum R^2 .

Figure 3 compares the estimates of RMSE for the training and the validation sets over several ANN trials over the dataset. One can conclude that the model is underfitted for a smaller number of neurons and overfitted for a large number of neurons. Figure 3 shows that the minimum value of the RMSE for both the training and the validation sets corresponds to four neurons in the first layer.

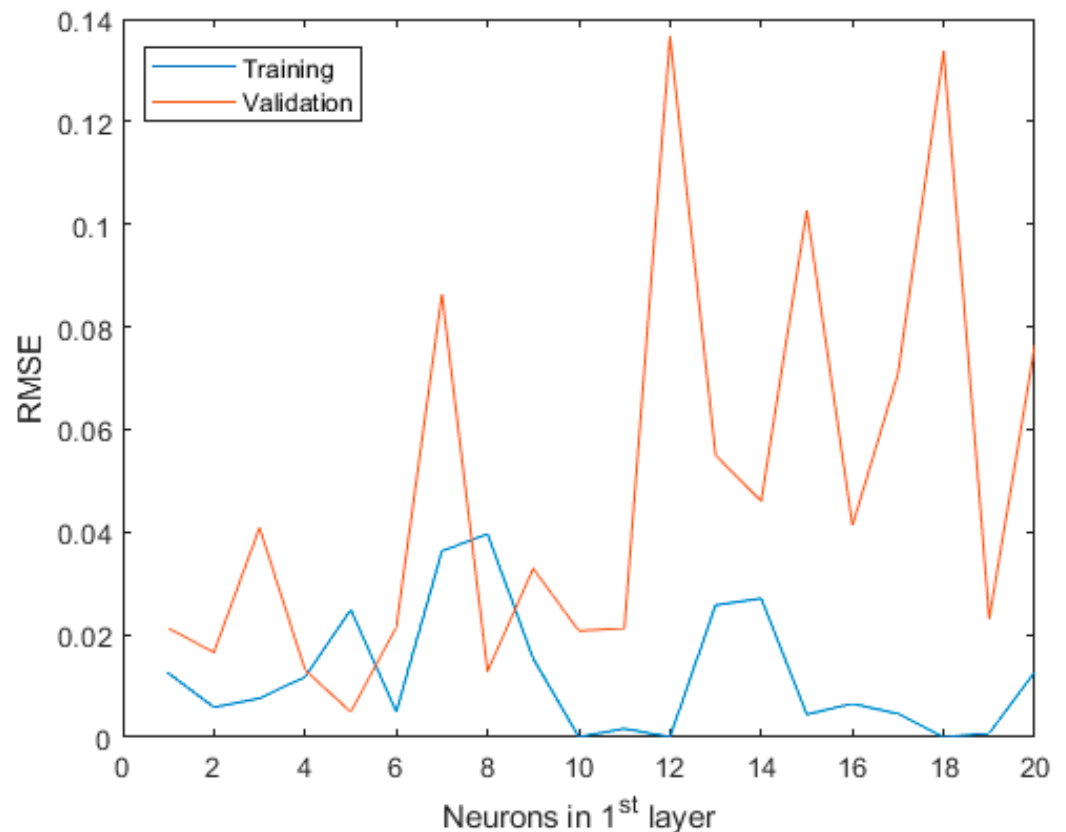


Figure 3. Estimates of various ANN models with one hidden layer.

The assessment of the ANN model for one hidden layer with four neurons in the absence of the second layer is shown in Figure 4. This figure indicates that the model predictions are too close to experiment values. The optimal value of RMSE (0.0452) and R^2 (0.965) corresponding to the whole set was obtained.

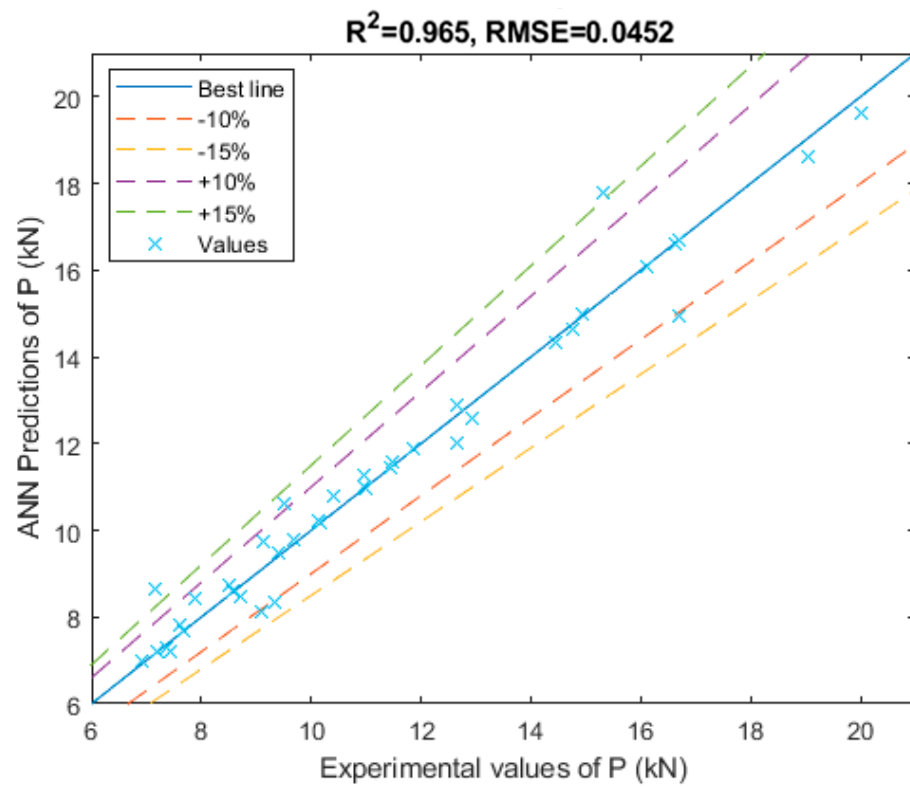


Figure 4. Assessment of the ANN model with four neurons in one hidden layer.

The variation of *RMSE* for the training and the validation sets as a function of the number of neurons in the second layer whereas preserving four neurons in the first layer is shown in Figure 5. It is proved that the minimum value of the *RMSE* for both the training and the validation sets corresponds to five neurons in the second layer.

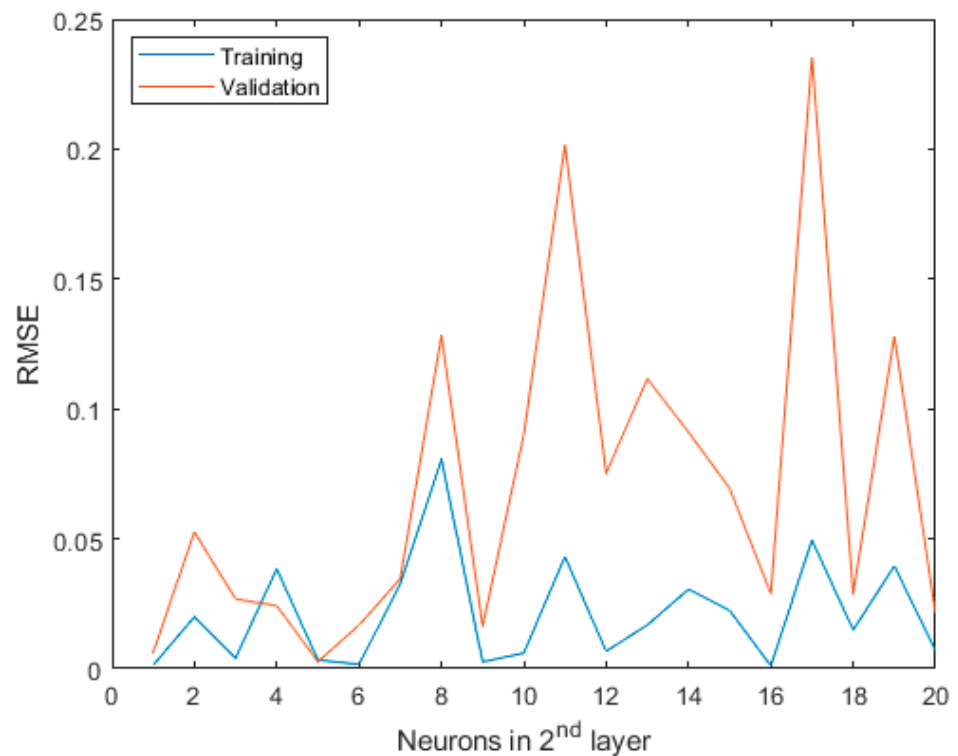


Figure 5. Estimates of various ANN models with two hidden layers.

The assessment of the ANN model with four neurons in the first hidden layer and five neurons in the second layer is shown in Figure 6. This figure indicates that this model delivers more accurate results compared to the ANN model with just one layer and compared the proposed mathematical equation obtained using MATLAB’s curve fitting procedure. When there were four neurons in the first HL and five neurons in the second HL, respectively, the optimal value of RMSE (0.0169) and R^2 (0.972) corresponding to the whole set was reached.

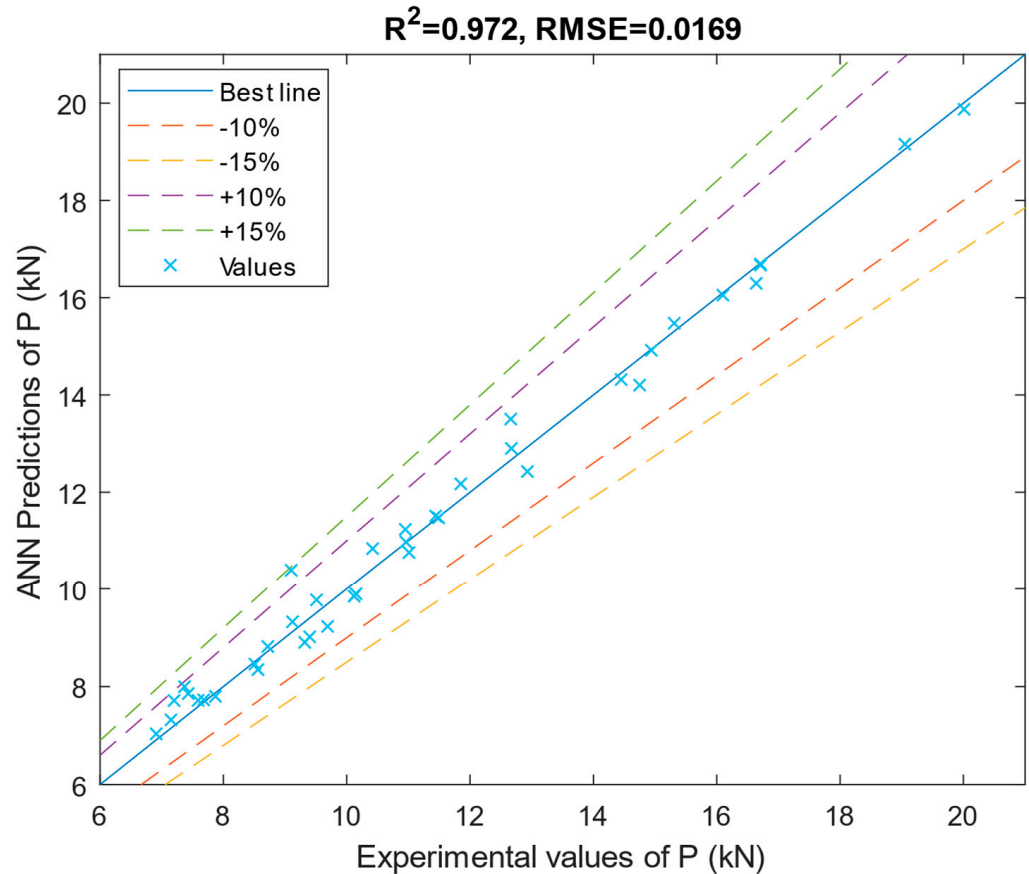


Figure 6. Assessment of the ANN model with 4 neurons in 1st hidden layer and 5 in the 2nd layer.

As a result, the assembly of the ANN model recommended in this study to calculate the bond strength of FRP sheets bonded to concrete is plotted in Figure 7.

4.3. Performance of ANN Model

Overfitting and Underfitting are the two main problems that occur in machine learning and degrade the performance of the models. Overfitting can happen whether because the model is too complex which memorizes very subtle patterns in the training data and does not generalize well or when the training data size is too small for the model complexity. Underfitting is faced when the model does not align well with the training data or generalize well to new data.

The performance of the developed model is evaluated with training dataset, validation dataset and testing dataset. Figure 8 shows that the error reduces after more epochs of training, but starts to increase on the validation dataset as the network starts overfitting the training data. The training stops after six consecutive increases in validation error, and the best performance is taken from the epoch with the lowest validation error. It is noted from Figure 8 that the mean square error for the training, validation and testing of datasets is very low; hence, the good performance of the proposed model is justified.

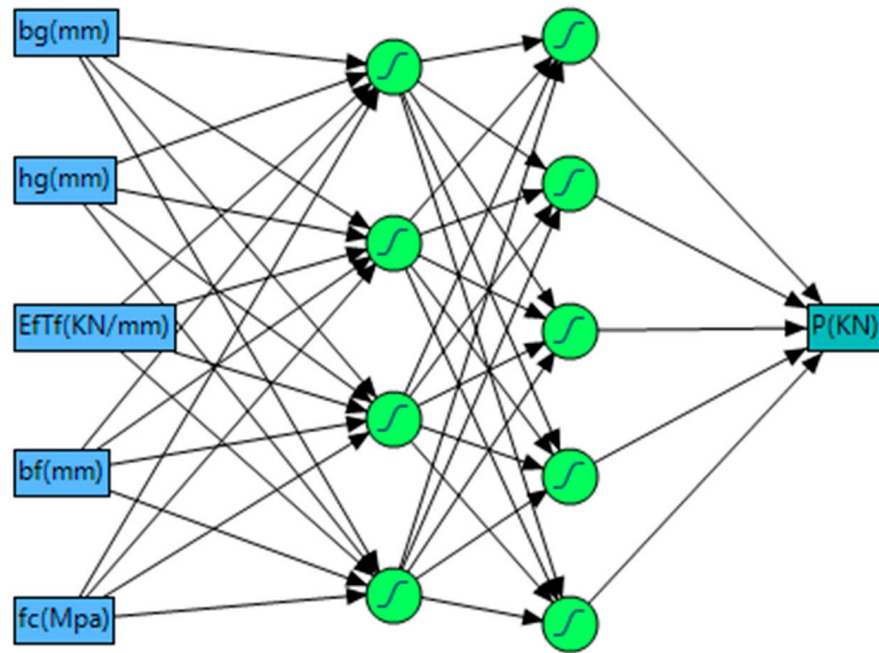


Figure 7. Structure of recommended ANN model.

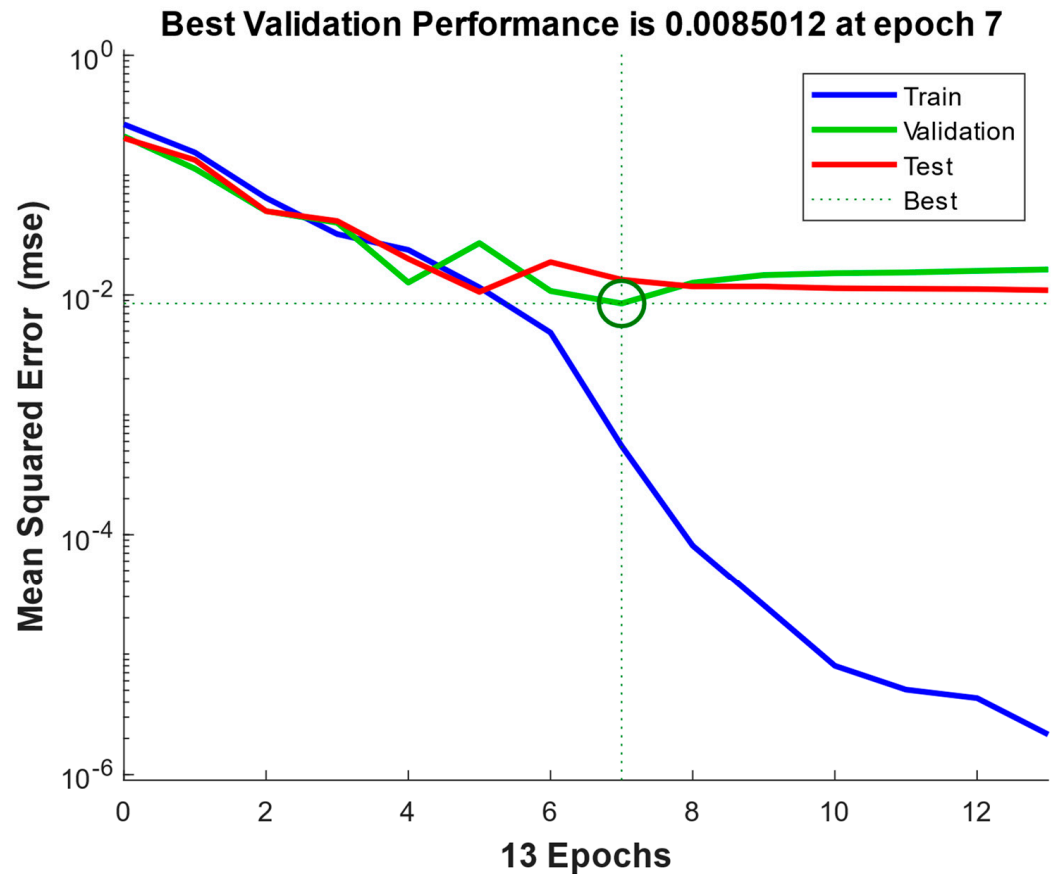


Figure 8. Variation of the mean square error as a function of the epochs.

5. Statistical Comparison

The testing outcomes employing the selected ANN model and the mathematical equation of the bond strength of FRP sheets bonded to concrete are shown in Tables 4 and 5, respectively, along with the outcomes of the static Analysis of Variance (ANOVA). Anal-

ysis Of Variance, written as ANOVA for short, is a statistical technique that compares sample populations based on their means and spread of the data. The model helps to answer the question of whether the means of two or more groups are significantly different. When analyzing the results of the one-way ANOVA test, two measures are used to make conclusions; the *p*-value and the comparison of F-test to F-critical value. The vital result of the model is the *p*-value, which only has meaning for the null hypothesis, stating all sample means are not significantly different (all groups have the same mean). In layman terms, the *p*-value can be interpreted as the level of confidence we have that the null hypothesis is a plausible model for the data.

Table 4. ANOVA outcomes for ANN estimates for the bond strength.

Groups	Count	Sum	Average			
Testing capacity (kN)	39	438.77	11.250			
mathematical equation Capacity (kN)	39	442.45	11.345			
Source of Variation	Sum of squares (SS)	Degrees of freedom (df)	Mean squares (MS)	<i>F</i>	<i>p</i> -value	<i>F_{crit}</i>
Between groups	0.17	1	0.17	0.0142	0.905	3.967
Within Groups	930.49	76	12.24			
Total	930.66	77				

Table 5. ANOVA outcomes for mathematical equation estimates for the bond strength.

Groups	Count	Sum	Average			
Testing capacity (kN)	39	442.45	11.34			
ANN model (kN)	39	441.79	11.33			
Source of Variation	Sum of squares (SS)	Degrees of freedom (df)	Mean squares (MS)	<i>F</i>	<i>p</i> -value	<i>F_{crit}</i>
Between groups	0.0056	1	0.0056	0.0005	0.983	3.967
Within Groups	870.9646	76	11.4601			
Total	870.9701	77				

For both ANN and mathematical estimations, the F-value is much lower than *F_{crit}*. ANN estimations showed a correctness probability of 98.3%, whilst mathematical estimates showed a correctness probability of 90.5%. As a result, it can be said that the suggested ANN and mathematical equations successfully prophesized the bond strength.

6. Parametric Study Employing ANN Equation

The bond strength of FRP sheets bonded on concrete via the ERBOG technique was predicted employing the expected ANN model during the parametric study. The groove’s width and depth, the tensile stiffness per width, the FRP sheet width, and the concrete compressive strength are the five factors employed in this parametric analysis. The specifics of these factors are shown in Table 6, when the effects of each factor were investigated while keeping the other factors constant.

The evolution of the bond strength as a function of the Groove’s width is given in Figure 9a. It was discovered that the evolution of the bond strength of FRP sheets bonded on concrete via EBROG technique as a function of the Groove’s width is not monotonous from 5 to 10 mm. Beyond 10 mm the bond strength decreases when the Groove’s width increases. The bond strength decreased by a factor of 1.32 when the Groove’s width raised from 10 to 15 mm.

Table 6. Factors employed for the parametric study.

Parameter	Constant Value	Investigated Counts
Groove’s width (mm)	7.89	5, 5.5, 6, 6.5, 7, 7.5, 8, 8.5, 9, 9.5, 10, 10.5, 11, 11.5, 12, 12.5, 13, 13.5, 14, 14.5, 15
Groove’s depth (mm)	9.87	5, 5.25, 5.5, 5.75, 6, 6.25, 6.5, 6.75, 7, 7.25, 7.5, 7.75, 8, 8.25, 8.5, 8.75, 9, 9.25, 9.5, 9.75, 10, 10.25, 10.5, 10.75, 11, 11.25, 11.5, 11.75, 12, 12.25, 12.5, 12.75, 13, 13.25, 13.5, 13.75, 14, 14.25, 14.5, 14.75, 15, 15.25, 15.5, 15.75, 16, 16.25, 16.5, 16.75, 17, 17.25, 17.5, 17.75, 18, 18.25, 18.5, 18.75, 19, 19.25, 19.5, 19.75, 20
Tensile stiffness per width (kN/mm)	37.54	10, 15, 20, 25, 30, 35, 40, 45, 50, 55, 60, 65, 70, 75, 80, 85, 90, 95, 100
FRP sheet width(mm)	45.79	20, 22, 24, 26, 28, 30, 32, 34, 36, 38, 40, 42, 44, 46, 48, 50, 52, 54, 56, 58, 60, 62, 64, 66, 68, 70
Concrete compressive strength (MPa)	34.76	20, 22, 25, 27, 30, 32, 35, 37, 40, 42, 45, 47, 50, 52, 55, 57, 60

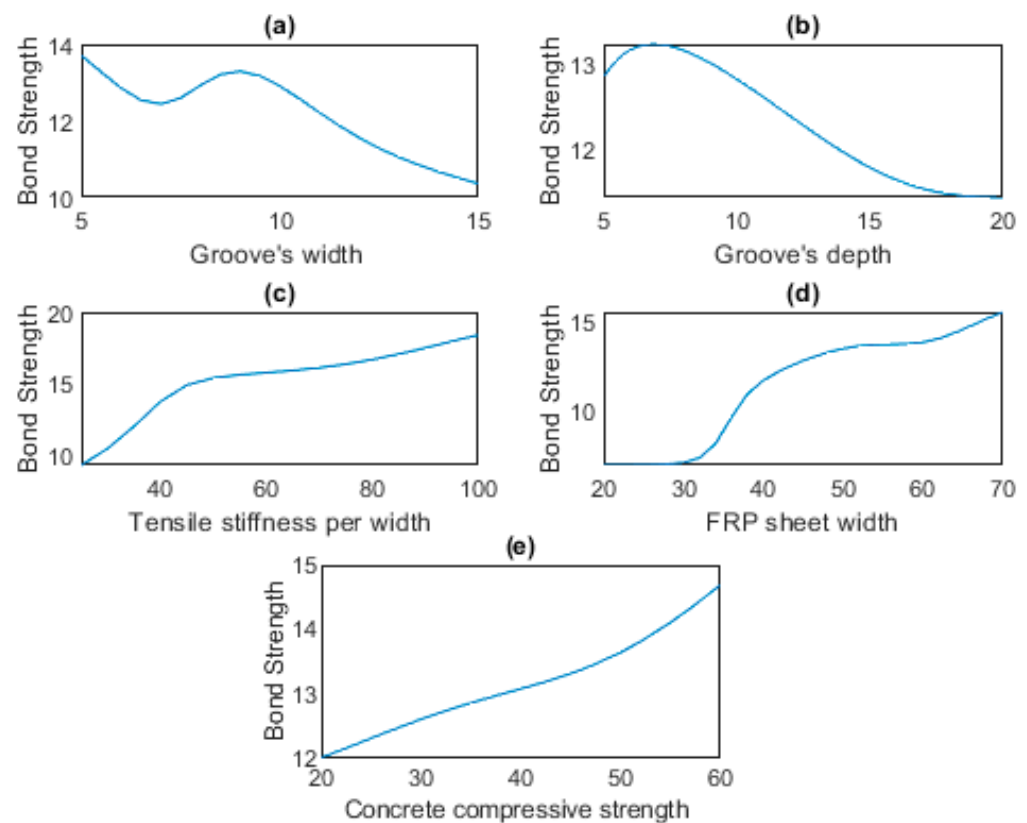


Figure 9. Parametric study outcomes for the FRP/Concrete bond strength.

Figure 9b depicts the influence of the Groove’s depth on the bond strength. It was noted that the bond strength increases for Groove’s depth in the interval [5 7.5] and decreases for a given value superior to 7.5 mm. The bond strength can reach 13.2 kN for Groove’s depth equal to 7.5 mm then climbs to 11.5 for Groove’s depth equal to 20 mm.

Figure 9c–e show, respectively, the variation of the bond strength as a function of the tensile stiffness per width, FRP sheet width, and the concrete compressive strength. It is observed from these figures that the tensile stiffness per width, the FRP sheet width, and

the concrete compressive strength have the same effect on the bond strength. This latter grew when these factors were raised. The bond strength of FRP sheets applied on concrete is improved by 2.6 kN when the concrete compressive strength is raised by 40 MPa. It was also seen that the bond strength rose by 72 percent when the tensile stiffness per width was augmented from 10 to 100 mm. The bond strength of the FRP sheet bonded to concrete improved by 200 percent when the FRP sheet width was raised from 20 to 70 mm.

7. Conclusions

The bond strength of FRP sheets bonded on concrete through EBROG was predicted by a mathematical equation using the MATLAB curve fitting method and by the ANN model. The suggested mathematical equation delivered good predictions compared to experimental results with $RMSE = 0.0641$, $R^2 = 0.954$. The ANN model, which included four neurons in each of the first layers and five neurons in the remaining layer, closely matched the outcomes of the experiment with $RMSE = 0.0169$, $R^2 = 0.972$. The validity of the presented Models was also strongly supported by one-way ANOVA statistical outcomes. This work shows that while even the regression method gives good predictions, an ANN model can be developed to increase the prediction accuracy even further. The parametric analysis employing the ANN model demonstrated that there is a considerable rise in the bond strength as the tensile stiffness per width, FRP sheet width and the concrete compressive strength are augmented. The evolution of the bond strength of FRP sheets applied on concrete via the EBROG technique as a function of the Groove's width and depth is not monotonous. The current work helps structural engineers by providing information for the design of FRP sheets applied to concrete via the EBROG technique.

Funding: This research was funded by Prince Sattam bin Abdulaziz University grant number PSAU/2023/01/25594.

Data Availability Statement: Data are contained within the article.

Acknowledgments: The authors extend their appreciation to Prince Sattam bin Abdulaziz University for funding this research work through the project number (PSAU/2023/01/25594).

Conflicts of Interest: The authors declare no conflicts of interest.

References

1. Dolati, S.S.K.; Malla, P.; Ortiz, J.D.; Mehrabi, A.; Nanni, A. Identifying NDT methods for damage detection in concrete elements reinforced or strengthened with FRP. *Eng. Struct.* **2023**, *287*, 116155. [\[CrossRef\]](#)
2. Castillo, E.; Griffith, M.; Ingham, J. Straight FRP anchors exhibiting fiber rupture failure mode. *Compos. Struct.* **2019**, *207*, 612–624. [\[CrossRef\]](#)
3. Moghaddas, A.; Mostofinejad, D.; Ilia, E. Empirical FRP-concrete effective bond length model for externally bonded reinforcement on the grooves. *Compos. Part B Eng.* **2019**, *172*, 323–338. [\[CrossRef\]](#)
4. Zhou, H.; Attard, T.L.; Dhiradhamvit, K.; Wang, Y.; Erdman, D. Crashworthiness characteristics of a carbon fiber reinforced dual-phase epoxy-polyurea hybrid matrix composite. *Compos. Part B Eng.* **2015**, *71*, 17–27. [\[CrossRef\]](#)
5. Attard, T.L.; Zhou, H. Damage absorption of high-impact structural systems using time-reaction of hybridized epoxy-polyurea interfaces. *Athens J. Technol. Eng.* **2016**, *3*, 71–88. [\[CrossRef\]](#)
6. Lu, X.Z.; Ye, L.P.; Teng, J.G.; Jiang, J.J. Meso-scale finite element model for FRP sheets/plates bonded to concrete. *Eng. Struct.* **2005**, *27*, 564–575. [\[CrossRef\]](#)
7. Seracino, R.; Raizal Saifulnaz, M.R.; Oehlers, D.J. Generic debonding resistance of EB and NSM plate-to-concrete joints. *J. Compos. Constr.* **2007**, *11*, 62–70. [\[CrossRef\]](#)
8. Sayed Ahmed, E.Y.; Bakay, R.; Shrive, N.G. Bond strength of FRP laminates to concrete: State-of-the-art review. *Electron. J. Struct. Eng.* **2009**, *9*, 45–61. [\[CrossRef\]](#)
9. Pan, J.; Wu, Y.F. Analytical modeling of bond behavior between FRP plate and concrete. *Compos. Part B Eng.* **2014**, *61*, 17–25. [\[CrossRef\]](#)
10. Vahedian, A.; Shrestha, R.; Crews, K. Effective bond length and bond behaviour of FRP externally bonded to timber. *Constr. Build. Mater.* **2017**, *151*, 742–754. [\[CrossRef\]](#)
11. *ACI 440.2R-17; Guide for the Design and Construction of Externally Bonded FRP Systems for Strengthening Concrete Structures.* American Concrete Institute: Farmington Hills, MI, USA, 2017.

12. Wu, Y.F.; Xu, X.S.; Sun, J.B.; Jiang, C. Analytical solution for the bond strength of externally bonded reinforcement. *Compos. Struct.* **2012**, *94*, 3232–3239. [[CrossRef](#)]
13. Grace, C.; Yang, Y.; Sneed, L. Fracture mechanics approaches to debonding behavior of reinforced concrete members with externally-bonded fiber reinforced polymer laminates. *ACI Spec. Publ.* **2012**, *286*, 99–118.
14. Karbhari, V.M.; Niu, H.; Sikorsky, C. Review and comparison of fracture mechanics based bond strength models for FRP-strengthened structures. *J. Reinf. Plast. Compos.* **2006**, *25*, 1757–1794. [[CrossRef](#)]
15. Ozbakkaloglu, T.; Saatcioglu, M. Tensile behavior of FRP anchors in concrete. *J. Compos. Constr.* **2009**, *13*, 82–92. [[CrossRef](#)]
16. Murad, Y. An experimental study on flexural strengthening of RC beams using CFRP sheets. *Int. J. Eng. Technol.* **2018**, *7*, 2075–2080. [[CrossRef](#)]
17. Ozbakkaloglu, T.; Fang, C.; Gholampour, A. Influence of FRP anchor configuration on the behavior of FRP plates externally bonded on concrete members. *Eng. Struct.* **2017**, *133*, 133–150. [[CrossRef](#)]
18. Al-Rousan, R.; Haddad, R.; Al-Halboni, A. Bond-slip behaviour between self-compacting concrete and carbon fibre-reinforced polymer sheets. *Mag. Concr. Res.* **2015**, *67*, 89–103. [[CrossRef](#)]
19. Haddad, R.; Al-Rousan, R.; Almasry, A. Bond-slip behavior between carbon fiber reinforced polymer sheets and heat-damaged concrete. *Compos. Part B Eng.* **2013**, *45*, 1049–1060. [[CrossRef](#)]
20. Irshidat, M.R.; Al-Saleh, M.H. Effect of using carbon nanotube modified epoxy on bond-slip behavior between concrete and FRP sheets. *Constr. Build. Mater.* **2016**, *105*, 511–518. [[CrossRef](#)]
21. Mostofinejad, D.; Hajrasouliha, M.J. Effect of concrete strength and groove dimensions on performance of grooving method to postpone debonding of FRP sheets in strengthened concrete beams. *IJST Trans. Civ. Eng.* **2013**, *37*, 219–232.
22. Mostofinejad, D.; Tabatabaei Kashani, A. Experimental study on effect of EBR and EBROG methods on debonding of FRP sheets used for shear strengthening of RC beams. *Compos. Part B Eng.* **2013**, *45*, 1704–1713. [[CrossRef](#)]
23. Mostofinejad, D.; Moghaddas, A. Bond efficiency of EBR and EBROG methods in different flexural failure mechanisms of FRP strengthened RC beams. *Constr. Build. Mater.* **2014**, *54*, 605–614. [[CrossRef](#)]
24. Hosseini, A.; Mostofinejad, D.; Hajjalilue Bonab, M. Displacement and strain field measurement in steel and RC beams using particle image velocimetry. *J. Eng. Mech.* **2014**, *140*, 04014086. [[CrossRef](#)]
25. Mostofinejad, D.; Mahmoudabadi, E. Grooving as alternative method of surface preparation to postpone debonding of FRP laminates in concrete beams. *J. Compos. Constr.* **2010**, *14*, 804–811. [[CrossRef](#)]
26. Mostofinejad, D.; Khozaei, K. Effect of GM patterns on ductility and debonding control of FRP sheets in RC strengthened beams. *Constr. Build. Mater.* **2015**, *93*, 110–120. [[CrossRef](#)]
27. Moshiri, N.; Tajmir-Riahi, A.; Mostofinejad, D.; Czaderski, C.; Motavalli, M. Experimental and analytical study on CFRP strips-to-concrete bonded joints using EBROG method. *Compos. Part B Eng.* **2019**, *158*, 437–447. [[CrossRef](#)]
28. Hosseini, A.; Mostofinejad, D.; Emami, M. Influence of bonding technique on bond behavior of CFRP-to-claybrick masonry joints: Experimental study using particle image velocimetry (PIV). *Int. J. Adhes. Adhes.* **2015**, *59*, 27–39. [[CrossRef](#)]
29. Mostofinejad, D.; Akhlaghi, A. Experimental investigation of the efficacy of EBROG method in seismic rehabilitation of deficient reinforced concrete beam-column joints using CFRP sheets. *J. Compos. Constr.* **2016**, *21*, 04016116. [[CrossRef](#)]
30. Adeli, H.; Yeh, C. Perceptron Learning in Engineering Design. *Microcomput. Civ. Eng.* **1989**, *4*, 247–256. [[CrossRef](#)]
31. Dimiduk, D.M.; Holm, E.A.; Niezgodna, S.R. Perspectives on the impact of machine learning, deep learning, and artificial intelligence on materials, processes, and structures engineering. *Integr. Mater. Manuf. Innov.* **2018**, *7*, 157–172. [[CrossRef](#)]
32. Dolbow, J.E.; Garikipati, K.; Park, H.S. *Computational Mechanics Vision and Future Challenges Workshop Report*; Technical Report; University of Michigan: Ann Arbor, MI, USA, 2019.
33. Shakiba, M.; Parson, N.; Chen, X.G. Modeling the effects of cu content and deformation variables on the high-temperature flow behavior of dilute Al-Fe-Si alloys using an artificial neural network. *Materials* **2016**, *9*, 536. [[CrossRef](#)]
34. Chojaczyk, A.A.; Teixeira, A.P.; Luis, C.; Cardoso, J.B.; Soares, C.G. Review and application of artificial neural networks models in reliability analysis of steel structures. *Struct. Saf.* **2015**, *52*, 78–89. [[CrossRef](#)]
35. Liu, G.R.; Xu, Y.G.; Wu, Z.P. Total solution for structural mechanics problems. *Comput. Methods Appl. Mech. Eng.* **2001**, *191*, 989–1012. [[CrossRef](#)]
36. Waszczyszyn, Z.; Ziemianski, L. Neural networks in mechanics of structures and materials—New results and prospects of applications. *Comput. Struct.* **2001**, *79*, 2261–2276. [[CrossRef](#)]
37. Tahir, Z.R.; Mandal, P. Artificial neural networks prediction of buckling load of thin cylindrical shells under axial compression. *Eng. Struct.* **2017**, *152*, 843–855. [[CrossRef](#)]
38. Cheng, J.; Li, Q.S. Reliability analysis of structures using artificial neural network based genetic algorithms. *Comput. Methods Appl. Mech. Eng.* **2008**, *197*, 3742–3750. [[CrossRef](#)]
39. Zhao, D.; Ren, D.; Zhao, K.; Pan, S.; Guo, X. Effect of welding parameters on tensile strength of ultrasonic spot welded joints of aluminum to steel—By experimentation and artificial neural network. *J. Manuf. Process.* **2017**, *30*, 63–74. [[CrossRef](#)]
40. Mathew, J.; Parfitt, D.; Wilford, K.; Riddle, N.; Alamaniotis, M.; Chroneos, A.; Fitzpatrick, M.E. Reactor pressure vessel embrittlement: Insights from neural network modelling. *J. Nucl. Mater.* **2018**, *502*, 311–322. [[CrossRef](#)]
41. Capuno, G.; Rimoli, J. Smart finite elements: A novel machine learning application. *Comput. Methods Appl. Mech. Eng.* **2019**, *345*, 363–381. [[CrossRef](#)]

42. Lefik, M.; Boso, D.P.; Schrefler, B.A. Artificial neural networks in numerical modeling of composites. *Comput. Methods Appl. Mech. Eng.* **2009**, *198*, 1785–1804. [[CrossRef](#)]
43. Chen, T.; Chen, H. Universal approximation to non-linear operators by neural networks with arbitrary activation functions and its application to dynamical systems. *IEEE Trans. Neural Netw.* **1995**, *6*, 911–917. [[CrossRef](#)] [[PubMed](#)]
44. Ajmani, A.; Kamthania, D.; Hoda, M.N. A comparative study on constructive and non-constructive supervised learning algorithms for artificial neural networks. In Proceedings of the 2nd National Conference (INDIACom), New Delhi, India, 8–9 February 2008; Bharati Vidyapeeth's Institute of Computer Applications and Management: New Delhi, India, 2008.
45. Mandal, S.; Sivaprasad, P.V.; Venugopal, S.; Murthy, K.P.N. Artificial neural network modeling to evaluate and predict the deformation behavior of stainless-steel type AISI 304L during hot torsion. *Appl. Soft Comput.* **2009**, *9*, 237–244. [[CrossRef](#)]
46. Chen, J.F.; Teng, J.G. Anchorage strength models for FRP and steel plates bonded to concrete. *J. Struct. Eng.* **2001**, *127*, 784–791. [[CrossRef](#)]
47. Ueda, T.; Dai, J. Interface bond between FRP sheets and concrete substrates: Properties, numerical modeling and roles in member behaviour. *Prog. Struct. Eng. Mater.* **2005**, *7*, 27–43. [[CrossRef](#)]
48. Biscaia, H.C.; Chastre, C.; Silva, M.A.G. Nonlinear numerical analysis of the debonding failure process of FRP-to-concrete interfaces. *Compos. Part B Eng.* **2013**, *50*, 210–223. [[CrossRef](#)]
49. Yum, J.Y.F.; Chow, T.W.S. A Weight Initialization Method for Improving training Speed in Feedforward Neural Network. *Neurocomputing* **2000**, *30*, 219–323. [[CrossRef](#)]
50. Horikawa, S.I.; Furuhashi, T.; Uchikawa, Y. On Fuzzy Modeling Using Fuzzy Neural Networks with the Back-Propagation Algorithm. *IEEE Trans. Neural Netw.* **1992**, *3*, 801–806. [[CrossRef](#)]
51. Zou, J.; Han, Y.; So, S.-S. Overview of Artificial Neural Networks. In *Artificial Neural Networks*; Humana Press: Totowa, NJ, USA, 2008; Volume 458, pp. 14–22.
52. LeCun, Y.A.; Bottou, L.; Orr, G.B.; Müller, K.R. Efficient Backprop. In *Neural Networks: Tricks of the Trade*; Springer: Berlin/Heidelberg, Germany, 2012; pp. 9–48.

Disclaimer/Publisher's Note: The statements, opinions and data contained in all publications are solely those of the individual author(s) and contributor(s) and not of MDPI and/or the editor(s). MDPI and/or the editor(s) disclaim responsibility for any injury to people or property resulting from any ideas, methods, instructions or products referred to in the content.